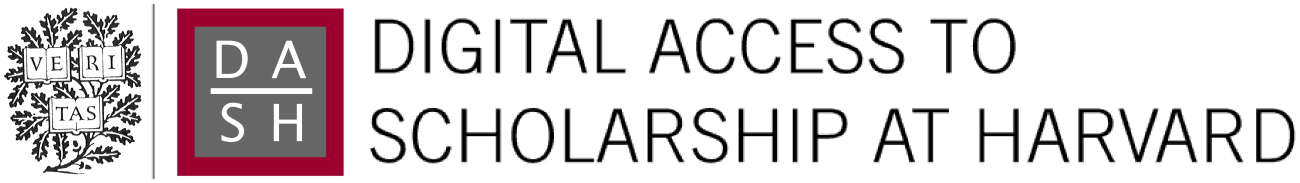

Bacterial recovery and recycling of tellurium from tellurium-containing compounds by Pseudoalteromonas sp. EPR3

For submission to Journal of Applied Microbiology

Bacterial recovery and recycling of tellurium from tellurium-containing compounds by *Pseudoalteromonas* sp. EPR3

William D. Bonificio #, David R. Clarke

School of Engineering and Applied Sciences, Harvard University, 29 Oxford St., Cambridge, MA 02138, United States

Running Title: Bacterial recovery of tellurium

Corresponding Author to whom inquiries should be addressed.

Mailing address: McKay 405, 9 Oxford St. Cambridge, MA 02138.

Email address: wdb@seas.harvard.edu

Keywords: *Pseudoalteromonas*; tellurium; tellurite; recycling; tellurium-containing compounds.

ABSTRACT

Aims: Tellurium based devices, such as photovoltaic (PV) modules and thermoelectric generators, are expected to play an increasing role in renewable energy technologies. Tellurium, however, is one of the scarcest elements in the earth's crust, and current production and recycling methods are inefficient and use toxic chemicals. This study demonstrates an alternative, bacterially mediated tellurium recovery process.

Methods and results: We show that the hydrothermal vent microbe *Pseudoalteromonas* sp. strain EPR3 can convert tellurium from a wide variety of compounds, industrial sources, and devices into metallic tellurium and a gaseous tellurium species. These compounds include metallic tellurium (Te^0), tellurite (TeO_3^{2-}), copper autoclave slime, tellurium dioxide (TeO_2), tellurium-based PV material (cadmium telluride, CdTe), and tellurium-based thermoelectric material (bismuth telluride, Bi_2Te_3). Experimentally, this was achieved by incubating these tellurium sources with the EPR3 in both solid and liquid media.

Conclusions: Despite the fact that many of these tellurium compounds are considered insoluble in aqueous solution, they can nonetheless be transformed by EPR3, suggesting the existence of a steady state soluble tellurium concentration during tellurium transformation.

Significance and impact: These experiments provide insights into the processes of tellurium precipitation and volatilization by bacteria, and their implications on tellurium production and recycling.

INTRODUCTION

In the last decade the unique optical and electronic properties of tellurium have been harnessed to create photovoltaic (PV) modules (Ullal and Roedern 2007) and high efficiency thermoelectric generators (Kraemer *et al.* 2011), rapidly increasing the element's demand. As a result, many reports have been published regarding tellurium's availability and its consequent impact on the use of cadmium telluride (CdTe) PVs and bismuth telluride (Bi_2Te_3) thermoelectric generators (Andersson 2000; Reiser *et al.* 2009; Patyk 2009; Zweibel 2010; Green 2011; Homm and Klar 2011; Amatya and Ram 2011; Candelise *et al.* 2012; Gaultois *et al.* 2013). Projections indicate that recycling tellurium could largely eliminate issues with scarcity (Marwede and Reller 2012), although the suggested methods are complex and rely on hazardous chemicals (Fthenakis and Wang 2004, 2006; Fthenakis 2004; Wang and Fthenakis 2005; Berger *et al.* 2010; Okkenhaug 2010). Additionally, even with the use of hazardous chemicals, 90% of tellurium can be lost employing current methods of tellurium recovery (Claessens and White 1993; Stafiej *et al.* 1999). In light of these facts, the United States Department of Energy (DOE) recognized that tellurium demand is projected to outpace supply. In its 2011 strategy report, the DOE classified tellurium as a 'near critical' element for the foreseeable future in terms of scarcity and importance to future energy technology (Bauer *et al.* 2011), outlining the importance of improvements in tellurium's efficient concentration, recovery, and recycling.

Tellurium is primarily produced as a byproduct of mining copper (Jennings 1971). It exists as impure tellurides (e.g., copper telluride, and silver telluride) with an abundance of 0.1 ppm in copper ore (Andersson 2000; Green 2009). Tellurium separation and purification is a complex process involving many tellurium intermediates, and the exact details vary from one refinery to another. One step used in the United States, the reduction of tellurium dioxide (TeO_2) to metallic tellurium (Te^0), requires a week-long, high temperature, high pressure autoclaving in concentrated hydrochloric acid with sulfur dioxide (W. Read, ASARCO, personal communication). Both concentrated hydrochloric acid and sulfur dioxide are hazardous, making alternative purification methods attractive from an environmental and safety vantage. Autoclave

slime, the effluent in processing tellurium from copper anode slime, contains tellurium, and has potential to be a major source for further tellurium recovery.

Bacterial-mediated approaches to tellurium recovery have not been extensively investigated, but have the potential to confer substantial advantages relative to present methods. Bacteria are currently used to separate a number of elements from their sources, most notably in the bioleaching of iron and copper from their ores (Olson *et al.* 2003; Rohwerder *et al.* 2003; Bosecker 2006) and remediating lead and cadmium from wastewater (Lovley and Coates 1997; Veglio and Beolchini 1997; Volesky 2001). In iron bioleaching, *Leptospirillum ferrooxidans* assists in mobilizing iron from ore bodies by oxidizing iron (II) (Sand *et al.* 1992). In water remediation, *Bacillus subtilis* biosorbs heavy metals on to its surface, removing them from waste effluent (Dostálek 2011). These processes, however, are not suitable for tellurium recovery: *L. ferrooxidans'* oxidation is reported to be limited to iron (Escobar *et al.* 2008), and biosorption is generally not specific to individual metals. Targeted tellurium recovery requires specificity for tellurium and activity over a wide range of tellurium concentrations.

Among the metals that are known to undergo a biogeochemical cycle, tellurium is probably least understood. It is generally considered toxic to bacteria because the soluble form, tellurite (TeO_3^{2-}), oxidizes thiols and produces reactive oxygen species (Deuticke *et al.* 1992; Albeck *et al.* 1998; Turner *et al.* 2001; Borsetti *et al.* 2005; Tremaroli *et al.* 2007). Bacteria are believed to relieve the stress from environmental tellurite by precipitating the tellurite as insoluble metallic tellurium (Te^0) and methylating it to a volatile tellurium species, that includes dimethyl telluride ($Te(CH_3)_2$) (Turner 2001; Basnayake *et al.* 2001; Araya *et al.* 2004; Swearingen *et al.* 2004; Pérez *et al.* 2007; Ollivier *et al.* 2008, 2011; Chasteen *et al.* 2009). In addition, the Challenger mechanism describes how tellurite biomethylation to dimethyl telluride occurs (Challenger 1945; Thayer 2002; Chasteen and Bentley 2003), but there is no consensus as to the mechanism of tellurite reduction to metallic tellurium. Although non-specific reduction by enzymes like nitrate reductases is considered a possibility (Avazéri *et al.* 1997; Sabaty *et al.* 2001), Calderón et al. report isolating a protein that reduces tellurium via

NADPH oxidation (Calderón *et al.* 2006). Concentration and conversion of tellurite to metallic tellurium is a critical step in the tellurium recovery process for production and recycling. There is only one group we are aware of that attempts to accomplish this using bacteria, where *Pseudomonas mendocina* was used. (Paknikar *et al.* 1997; Rajwade and Paknikar 2003)

Hydrothermal vent bacteria are of particular interest to us for tellurium recovery because vent chimneys are among the world's richest sources of tellurium (ζ_{Te} = 50 ppm) (Butler *et al.* 1999; Green 2009). It has also been suggested that under the combination of high pressures (250 atm) and temperature (400°C) tellurium (from the vent fluid) substitutes for sulfur in vent walls (Butler *et al.* 1999). The microbes that inhabit these vents are exposed to high concentrations of tellurium (Yoon *et al.* 1990). Vent bacteria from the genus *Pseudoalteromonas* are relatively resistant to tellurium (Rathgeber *et al.* 2002, 2006; Holden and Adams 2003), possibly evolving the ability to use tellurite as a terminal electron acceptor during metabolism (Csotonyi *et al.* 2006; Baesman *et al.* 2007). For this reason, after investigating various other vent bacteria to use in our study (data not shown), we chose to focus on *Pseudoalteromonas* sp. strain EPR3 (DSMZ 28475).

By investigating its response to tellurium we found that EPR3 transformed a variety of tellurium containing compounds including cadmium telluride, bismuth telluride, autoclave slime (a waste product of tellurium production), and tellurium dioxide (an intermediate in tellurium production) to metallic tellurium and a gaseous tellurium species. These compounds are considered insoluble (Schweitzer and Pesterfield 2010), but our experiments suggest that EPR3 acts on a dissolved tellurium species to precipitate and methylate tellurium from these compounds. These results demonstrate the potential for bacteria in tellurium recovery.

MATERIALS AND METHODS

Media and reagents. The following tellurium sources were used in this study, metallic tellurium (Sigma-Aldrich, St. Louis, USA), potassium tellurite (Sigma-Aldrich, St.

Louis, USA), tellurium dioxide (Spectrum Laboratory Products, Inc., New Brunswick, USA), bismuth telluride (Crescent Chemical Co., Inc., Islandia, USA), cadmium telluride (Strem Chemicals, Inc., Newburyport, USA), and copper autoclave slime (obtained from the Freeport-McMoRan Copper and Gold El Paso, Tx refinery). The growth media for EPR3 was artificial seawater (ASW) (Vetriani *et al.* 2005) which was sterilized by autoclaving at 121°C for 15 min. For solid culture, ASW was solidified using 1.5% (wt/vol) agar and added to 10 cm diameter by 1.5 cm high plates. EPR3 was donated by C. Vetriani who isolated it from hydrothermal vent fluid in the East Pacific Rise (Vetriani *et al.* 2005).

Approximation of tellurite's inhibitory concentration. The approximate inhibitory concentration of tellurite was determined by aerobically growing EPR3 in varying concentrations of autoclaved tellurite-amended ASW and observing the maximum tellurite concentration at which cell growth occurred. 0.8 mmol l^{-1}, 0.5 mmol l^{-1}, 0.3 mmol l^{-1}, and 0.1 $mmol^{-1}$ tellurite solutions of ASW were prepared by dissolving potassium tellurite in ASW. EPR3 was inoculated (1:100 dilution of fully grown culture, OD_{600nm} = 0.7) into each capped test tube liquid sample and incubated at 37°C for 72 h with continued shaking. Cell growth was observed visually by sample turbidity and a darkening of cells resulting from metallic tellurium precipitation. Sterile tellurite-amended ASW controls at the above mentioned tellurite concentrations were also made. In subsequent experiments concentrations of tellurite were chosen to be slightly less than the observed approximate inhibitory concentration.

Assay of dissolved tellurium concentration with time. EPR3's ability to transform tellurite was demonstrated by incubating EPR3 with a known concentration of tellurite in liquid media, and measuring the decrease in the soluble tellurium concentration over time. Four 15 ml conical tube samples containing 5 g of sterile liquid ASW were amended with 0.09 mmol l^{-1} potassium tellurite. Three samples were inoculated with EPR3 (1:100 dilution) and the other remained sterile. All of the samples were capped and incubated aerobically at 37°C with continued shaking at 70 rpm. Approximately every 24 h for 4 days after inoculation, the samples were centrifuged (9000 g, 25°C) to separate any cells and solid tellurium from the supernatant ASW of

the liquid culture. 50 µL of the supernatant from each sample was pipetted, weighed, and combined with 5 g of 2% trace metal free nitric acid in preparation for ICP-MS (inductively coupled plasma – mass spectrometry) analysis.

Tellurium precipitation and volatilization assay on solid media. Precipitation and volatilization of tellurite, metallic tellurium, tellurium dioxide, autoclave slime, cadmium telluride, and bismuth telluride on solid ASW was determined by growing EPR3 on plates with powders of these compounds sprinkled near the center, then measuring gaseous tellurium and metallic tellurium production by ICP-MS and confocal Raman spectroscopy, respectively. A 0.1 mmol l^{-1} tellurite agar plate was prepared by dissolving potassium tellurite in sterile liquid ASW, and then solidified with agar and inoculated with EPR3. For the other, insoluble, tellurium compounds, approximately 0.5 g of metallic tellurium, tellurium dioxide, and bismuth telluride, and approximately 0.1 g of copper autoclave slime and cadmium telluride, were added to the center of ASW plates that had been inoculated with 100 µl of a fully grown culture of EPR3 (OD_{600nm} = 0.7). Identical plates, containing the tellurium compounds, but absent of EPR3, were made as controls. They remained completely unchanged through the course of our experiments and no movement of the tellurium sources was noted. Photographs were taken of each plate before and after 48 h of incubation at 37°C. The tellurite plate was aged an additional 120 h before a final photograph was taken. Adobe Photoshop CS3 software was used to match the brightness, contrast, and saturation of photos between aged and unaged plates. The matching was applied equally to all parts of the images. On the plates with cells, areas of cell growth that blackened indicative of tellurium precipitation were cut with a razor blade from the agar and extracted for analysis. Confocal Raman spectroscopy (LabRAM Aramis Horiba Jobin YVON, 532nm laser) was performed on these samples, the controls, and reference samples of the pure tellurium compounds. In this method, a region of interest was identified in the confocal optical image. Then, the microscope laser beam was focused onto a feature and the Raman spectrum recorded, typically using a micron diameter beam. Raman was chosen because of its ability to unambiguously distinguish the presence of metallic tellurium. Metallic tellurium exhibits very distinctive major Raman peaks at 120.4 ± 0.5 cm^{-1} and 140.7 ± 0.5 cm^{-1} (Pine and Dresselhaus 1971), while tellurium dioxide is characterized

by major Raman peaks at 121 cm^{-1}, 152 cm^{-1}, 174cm^{-1}, and 199 cm^{-1} (Mirgorodsky *et al.* 2000). None of the other controls, including the tellurite dissolved in ASW, exhibited any Raman signal between 100 cm^{-1} and 200 cm^{-1}. The Raman spectra of metallic tellurium, tellurium dioxide, and 0.1 mmol l^{-1} tellurite in ASW agar are shown in Figure 1.

We were not able to quantify the sensitivity of the Raman measurements because it is a function of many variables which are difficult to control, especially those associated with light scattering, such as surface roughness and crystallographic orientation. Nevertheless, Raman spectra with good signal to noise were obtainable, and in each case the identification was unambiguous.

A gaseous tellurium species was detected by loading the cut and extracted agar samples with bacterial tellurium precipitation into the gas sampling chamber of an ICP-MS (Agilent Technologies 7700x). In this configuration the head space above the samples is carried to the ICP-MS and sampled for tellurium to determine the existence of gaseous tellurium, likely to include dimethyl telluride based on previous studies, along with other volatile tellurium compounds that are known to form (Araya *et al.* 2004; Swearingen *et al.* 2004; Ollivier *et al.* 2008, 2011). A mass-to-charge ratio of 125 was used to detect tellurium (Te^{125}). The tellurium response from EPR3 with the various tellurium compounds was compared to controls of the tellurium sources on sterile ASW plates. For our system, this detectability was approximately 100 to 1000 times smaller than the values in volatilized tellurium samples (our ICP-MS has the ability to detect as low as 10^{-12} g of tellurium).

Dissolved tellurium compound concentration assay. The solubility of each tellurium compound in ASW at 37°C was calculated by adding each compound to a known mass of sterile liquid ASW, and using ICP-MS to analyze the concentration of dissolved tellurium. Approximately 0.1 g of metallic tellurium, tellurium dioxide, autoclave slime, cadmium telluride, and bismuth telluride were added to 15 ml conical tubes containing 5 g of sterile liquid ASW. All samples, including a sterile ASW control, were capped and incubated at 37°C for 48 h with continued shaking. Next, the samples were centrifuged (9000 g, 25°C) to isolate the media with dissolved tellurium from solid tellurium compounds. A known mass of the supernatant ASW was removed and diluted

with a known mass of 2% trace metal free nitric acid to prepare for ICP-MS analysis. The ASW control contained no detectable concentration of tellurium.

Tellurium precipitation assay in liquid media. Precipitation of tellurium from tellurite, metallic tellurium, and tellurium dioxide in liquid ASW was observed by inoculating ASW containing these tellurium compounds with EPR3 and taking photographs and measuring visible light absorption. Approximately 0.1 g of metallic tellurium and tellurium dioxide, and 0.1 mmol l^{-1} tellurite were added to capped tubes of sterile ASW, with 3 replicates of each. These samples, including a sample of tellurium-free ASW, were inoculated with EPR3 (1:100 dilution of fully grown culture). Then, along with a sterile ASW control, the samples were aerobically incubated at 37°C with continued shaking. At various time points, indicated in the results section, the samples were removed for photographic recording and UV-vis absorption spectrophotometry (Thermo Scientific Helios Omega) measurements. In preparation for the spectrophotometry, 500 µL of each sample was removed and added to a plastic cuvette. After measuring the optical absorption, the solution was added back into the samples. Care was taken to avoid any biological contamination during these transfers. The sterile ASW control was taken as the baseline absorbance before each absorbance measurement. The absorbance was measured between 450 – 800 nm and integrated over this range for comparison between samples over time.

Liquid ICP-MS analysis assay. Liquid ICP-MS (inductively coupled plasma – mass spectrometry, Agilent Technologies 7700x) analysis was able to detect the concentration of nominal dissolved tellurium in liquid samples with high sensitivity (parts per trillion concentrations). A range of tellurium concentrations (blank – 1 ppm) were used as ICP-MS calibration standards, and indium and bismuth were used as ICP-MS internal standards. A mass-to-charge ratio of 125 was used to detect dissolved tellurium concentrations, which had a detectability limit of ~20 nM (calculated based on blank samples that were included in each run compared to calculated tellurium concentrations in standards). The dissolved tellurium concentrations of ASW samples were calculated based on the concentration results from ICP-MS analysis and the known masses of ASW and 2% trace metal free nitric acid in each sample. When

measuring the concentration of tellurium from incubated bismuth telluride, the internal standard consisted only of indium, and did not include bismuth.

RESULTS

EPR3 response to tellurite

Our preliminary work indicated that tellurite had an inhibitory concentration of approximately 0.3 mmol l^{-1} on EPR3. When EPR3 was exposed to soluble tellurite on solid culture, the bacterial lawn darkened and a distinctive garlic odor was noticed. The darkening is characteristic of optical absorption by metallic tellurium. This was substantiated using confocal Raman spectroscopy to show that the visible precipitate was metallic tellurium (Fig 2.) The garlic odor, which is characteristic of bacterial volatilization of tellurite to a gaseous tellurium species (Chasteen and Bentley 2003), was confirmed by analyzing the bacterial lawn's headspace for tellurium using ICP-MS (Fig. 3). On the solid agar, those portions of the bacterial lawn where metallic tellurium precipitated and became dark brown after 48 h gradually faded to a lighter brown after an additional 120 h (Fig 4). As the dark color of the bacterial lawn faded there was a concurrent decrease in the Raman intensity of the metallic tellurium Raman spectrum until when there was no color remaining, no Raman peaks were distinguishable. In addition, measurements of the dissolved tellurium concentration in tellurite-amended liquid ASW decreased 93% when inoculated with EPR3 (Fig. 5). This loss was attributed to the precipitation of tellurite to metallic tellurium and the subsequent volatilization of a gaseous tellurium species. The sterile tellurite controls exhibited no turbidity, darkening, or decrease in tellurium concentration in the sample from either cell growth or metallic tellurium precipitation as measured by spectrophotometry and ICP-MS. In addition, no volatile tellurium species was detected in the headspace of any of the controls measured for figure 3.

EPR3 response to metallic tellurium and tellurium dioxide

When fine metallic tellurium particles were added to the center of a plate of agar inoculated with EPR3, metallic tellurium was found well away from the original tellurium source (Fig. 4) as evidenced by confocal Raman spectroscopy (Fig. 2). In addition, ICP-MS analysis showed these bacteria evolved volatile tellurium (Fig. 3). To confirm the possibility of the dissolution of metallic tellurium, we added metallic tellurium to sterile liquid ASW. After 48 h, the amount of dissolved tellurium, measured using ICP-MS, was 0.038 mmol l^{-1} (Table 1).

In order to test EPR3's response to tellurium dioxide, tellurium dioxide was added to a plate with EPR3, and incubated for 48 h. The bacterial lawn immediately adjacent to the tellurium dioxide became dark brown in color, indicative of precipitated tellurium, and ranged from dark brown to light brown with increasing distance from the tellurium dioxide (Fig. 4). Confocal Raman spectroscopy and ICP-MS confirmed the presence of metallic tellurium (Fig. 2) and a gaseous tellurium species (Fig. 3) in this sample. It was unclear, however, if the bacteria in contact with tellurium dioxide were directly reducing it, or if the tellurium dioxide was passing through an intermediate soluble phase, such as tellurite, before it was reduced. Tellurium dioxide in liquid ASW dissolved slightly (Table 1), therefore, it is possible that dissolved tellurium diffused through the agar plate and was precipitated by the bacteria well away from the tellurium dioxide source.

EPR3 response to tellurium compounds in liquid media

EPR3's response to tellurite, metallic tellurium, and tellurium dioxide in liquid media was measured over 168 h using sequentially recorded photographs and visible light spectrophotometry. As with the solid media, EPR 3 darkened first and then faded gradually to a lighter brown (Fig. 6). As both the bacterial population and the effect of tellurium on them could not be separated, the spectrophotometry data represents the combined effect. Even so, the photographs show that EPR3 produced tellurium within the first 24 h of growth. Controls of each tellurium compound in sterile ASW showed no change in optical absorbance over the course of the measurement time.

EPR3 for recovery of tellurium from devices and autoclave slime

Normally an effluent from copper and tellurium production, autoclave slime is a potential source for tellurium recovery using bacteria. To evaluate EPR3's interaction with the slime, a similar set of experiments to metallic tellurium and tellurium dioxide were performed. Autoclave slime from Freeport-McMoRan in the form of an insoluble dried powder was added to the center of a dish plated with EPR3, and incubated. After 48 h, the bacterial lawn darkened to a light brown in a similar manner characteristic of tellurium precipitation (Fig. 7). The presence of both metallic tellurium (Fig. 7) and gaseous tellurium (Fig. 3) in bacteria away from the autoclave slime was again confirmed using confocal Raman spectroscopy and ICP-MS. Slight dissolution of the slime also occurred in liquid ASW, reaching a tellurium concentration of 0.066 mmol l^{-1} (Table 1).

To demonstrate the use of EPR3 for PV and thermoelectric waste recycling, large pieces of cadmium telluride and bismuth telluride were exposed to EPR3 on agar plates, and incubated for 48 h. During that time parts of the bacterial lawn around the particles darkened, again indicative of metallic tellurium precipitation (Fig. 7). The presence of metallic tellurium was again confirmed with confocal Raman spectroscopy (Fig. 7). In addition, a gaseous tellurium species was detected in the headspace above these bacteria using ICP-MS (Fig 3). Incubating cadmium telluride and bismuth telluride in liquid ASW and measuring the amount of dissolved tellurium after 48 h confirmed a soluble tellurium species' presence from both compounds (Table 1). Only 0.001 mmol l^{-1} tellurium was detected after 48 h from cadmium telluride though (compared to 0.037 mmol l^{-1} soluble tellurium from bismuth telluride), indicating that EPR3 was active in transforming soluble tellurium at low concentrations.

DISCUSSION

Despite the chemical differences between the solid tellurium compounds used as sources, EPR3 was found to be effective in converting each of them to metallic tellurium and a gaseous tellurium species. The conversion occurred at bacterial cells located on agar plates a distance from the surface of the solid sources, as evidenced by the

precipitation of metallic tellurium, confirmed by Raman spectroscopy, well away from the powders used as the sources. It is concluded that all the solids exhibit some solubility and that the tellurium is transported as a soluble ion from the source particles to the bacterium which, in turn, acts to reduce the anion to metallic tellurium as well as a gaseous tellurium species, detectable by Raman and ICP-MS, respectively. It is likely, based on the circumneutral pH's we have measured and the tellurium Pourbaix diagram (Jennings 1971), that the soluble anion is the tellurite oxyanion, but the identity of the gaseous tellurium species has yet to be established. Based on the distinctive garlic odor accompanying the bacterial action, however, we believe it to include dimethyl telluride.

Based on our experimental observations we propose that several inter-related and coupled processes occur during the bacterial speciation of tellurium. These are illustrated schematically in figure 8. When the solid tellurium sources are added to agar and liquid ASW, they dissolve until the solubility limit is reached, local equilibrium is established and no further net dissolution occurs. This solubility, given by the reaction rate constant, is low and, indeed, tellurium solids are generally considered to be insoluble in aqueous solutions (Schweitzer and Pesterfield 2010). However, when EPR3 is present, the soluble ion diffuses across the cell membrane. Inside the cell, two coupled reactions occur concurrently. One, we infer from our data, is a reversible reduction-oxidation reaction between the tellurite ion and metallic tellurium that is responsible for the internal bacterial precipitation of metallic tellurium. The other we suggest, is methylation by the Challenger mechanism to a gaseous tellurium species that can diffuse out through the cell membrane and either volatize to the air atmosphere or reform the soluble tellurite ion in the solution.

After an initial incubation period, while there remains a solid tellurium source and the cells reproduce, we believe that a steady state is established. During this steady state the soluble tellurite oxyanion formed by dissolution of the source is transported and converted by the cells to metallic tellurium and, a yet unidentified, gaseous tellurium species, most likely including dimethyl telluride. In essence, in steady state the solid dissolution rate is equal to the volatilization rate buffered by the precipitated metallic

tellurium produced by the cell, with the rates being dependent on temperature, pH, partial pressure of oxygen, and the cell concentration. Once the source of tellurium is consumed, the metallic tellurium buffer in the cells is depleted and the overall reaction ceases. The changes observed on the agar plates are visible evidence of these reactions: the darkening due to the precipitation of metallic tellurium at distances away from the powder sources and the subsequent lightening in color as the amount of tellurium decreases until none remains and the agar returns to its initial color. The observed color changes when the bacterial reaction occurs in the liquid medium is also consistent with this overall reaction although less vivid.

It is possible that other soluble and volatile tellurium compounds, not shown in figure 8, may also be present and contribute to the overall tellurium cycling. However, the similarity of EPR3's response to the different solid compounds, leads us to conclude that EPR3 is acting on the same tellurium containing molecule which we believe is the tellurite oxyanion. This conclusion can be applied to other tellurium compounds not discussed here, such as bacterial tellurate (TeO_4^{2-}) (Araya *et al.* 2004; Csotonyi *et al.* 2006; Baesman *et al.* 2007), and telluric acid ($Te(OH)_6$) (W.D. Bonificio and D.R. Clarke, unpublished data) precipitation and volatilization, as well as anecdotal studies on tellurium transformation by mammals ingesting metallic tellurium (Chasteen *et al.* 2009). It is also consistent with the work of Ollivier et. al. (2011) which shows that a marine yeast precipitated metallic tellurium from a biologically evolved gaseous tellurium species. We also suggest that there is a concurrent reaction between the gaseous tellurium species being oxidized to tellurite and precipitating as metallic tellurium. This reversible reaction of gaseous tellurium species to tellurite is represented in Figure 8 by the dotted arrows. It is shown dotted because of our uncertainty of the actual mechanism.

In order for some of the tellurium compounds to dissolve, a 4 or 6 electron oxidation process is required, for instance, to convert Te^{2-} in tellurides and Te^0 in metallic tellurium to Te^{4+} in tellurite. We propose that molecular oxygen provides the necessary oxidization potential to transform these compounds. Our observations that metallic tellurium precipitates faded away faster on agar than in liquid media supports

this. On agar, the metallic tellurium is exposed to more oxygen, which favors dissolution to tellurite. Consequently, this tellurite is converted to a gaseous tellurium species and leaves the system faster than in samples exposed to less oxygen. This hypothesis is consistent with conclusions from Ollivier et. al. (2011) that aeration increases volatile tellurium formation and inhibits metallic tellurium formation in a marine yeast.

Alternatively, it is possible that the tellurium compounds, especially those in liquid media which are exposed to less oxygen and more reduced carbon, are being reduced to hydrogen telluride, and this is the compound which the bacteria act upon. However, no volatile tellurium, including hydrogen telluride, was detected by ICP-MS from the headspace of sterile tellurium amended ASW plates. For this reason we believe that this alternative is less likely.

Finally, irrespective of whether bacterial transformation of tellurite is a detoxification strategy or an 'unintended' byproduct of cellular reducing agents, more work is necessary to understand the complex interactions, including the enzymatic reactions, between bacteria and tellurium. Despite this we have demonstrated that EPR3 may be a useful bacterium in the recovery of tellurium because it is shown to be a versatile bacterium in the reduction and methylation of tellurium from a wide variety of solid tellurium compounds. This includes tellurium compounds used in renewable energy technologies, such as cadmium telluride photovoltaics and bismuth telluride thermoelectrics, as well as those used in the production of tellurium, such as autoclave slime and tellurium dioxide. Based on the observation that precipitation of metallic tellurium occurs in cells located well away from its sources in agar, it is concluded that some soluble tellurium species, likely to include the tellurite oxyanion, forms despite the reported insolubility of the solid sources, and diffuses to the cells. There the soluble tellurium is taken up by EPR3, precipitating metallic tellurium within the cell and more slowly converting, possibly by the Challenger mechanism, to a volatile tellurium species that diffuses out of the cell and escapes.

Interestingly, EPR3 shows resilience to the soluble tellurite oxyanion at concentrations of 0.3 mmol l^{-1}, significantly higher than reported in vent fluid (Yoon *et al.*

1990). Consequently, there is potential in using EPR3 to recover tellurium industrially, bypassing some of the existing processing steps, and, possibly, also in recycling. This will involve handling the volatized tellurium species and, in the case of processing cadmium telluride, special care in capturing the highly toxic dimethylcadmium (Strem Chemicals Inc.; Thayer 2002) if any were to evolve. Further research into purities, yields, and flow-through processes are clearly needed, but EPR3 and possibly other vent bacteria show considerable promise for both higher efficiency tellurium recovery and simpler processing.

ACKNOWLEDGEMENTS

This work was initiated with a grant from the Harvard University Center for the Environment and completed with funding from the Office of Naval Research under Grant No. N00014-11-1-0894.

We are grateful to C. Vetriani for providing the bacteria used in this study and B. Wesstrom (Freeport-McMoRan) for providing the autoclave slime. We thank P. Girguis for his advice, and A. Veil, A. Lorber, R. Zhang, A. Faux, and A. Cummings for their assistance.

CONFLICT OF INTEREST

No conflict of interest declared.

REFERENCES

Albeck A, Weitman H, Sredni B, Albeck M (1998) Tellurium compounds: Selective inhibition of cysteine proteases and model reaction with thiols. *Inorg Chem* **37**(8), 1704–1712.

Amatya R, Ram RJ (2011) Trend for thermoelectric materials and their earth abundance. *J Electron Mater* **41**(6), 1011–1019.

Andersson BA (2000) Materials availability for large-scale thin-film photovoltaics. *Prog Photovoltaics Res Appl* **8**(May 1999), 61–76.

Araya MA, Swearingen JW, Plishker MF, Saavedra CP, Chasteen TG, Vásquez CC (2004) *Geobacillus stearothermophilus* V *ubiE* gene product is involved in the evolution of dimethyl telluride in *Escherichia coli K-12* cultures amended with potassium tellurate but not with potassium tellurite. *J Biol Inorg Chem* **9**(5), 609–615.

Avazéri C, Turner RJ, Pommier J, Weiner JH, Giordano G, Verméglio A (1997) Tellurite reductase activity of nitrate reductase is responsible for the basal resistance of Escherichia coli to tellurite. *Microbiology* **143**(4), 1181–1189.

Baesman SM, Bullen TD, Dewald J, Zhang D, Curran S, Islam FS, Beveridge TJ, Oremland RS (2007) Formation of tellurium nanocrystals during anaerobic growth of bacteria that use Te oxyanions as respiratory electron acceptors. *Appl Environ Microbiol* **73**(7), 2135–2143.

Basnayake RST, Bius JH, Akpolat OM, Chasteen TG (2001) Production of dimethyl telluride and elemental tellurium by bacteria amended with tellurite or tellurate. *Appl Organomet Chem* **15**(6), 499–510.

Bauer D, Diamond D, Li J, McKittrick M, Sandalow D, Telleen P (2011) “U.S. Department of Energy critical materials strategy.” (U.S. Department of Energy)

Berger W, Simon F-G, Weimann K, Alsema EA (2010) A novel approach for the recycling of thin film photovoltaic modules. *Resour Conserv Recycl* **54**(10), 711–718.

Borsetti F, Tremaroli V, Michelacci F, Borghese R, Winterstein C, Daldal F, Zannoni D (2005) Tellurite effects on *Rhodobacter capsulatus* cell viability and superoxide dismutase activity under oxidative stress conditions. *Res Microbiol* **156**(7), 807–813.

Bosecker K (2006) Bioleaching: metal solubilization by microorganisms. *FEMS Microbiol Rev* **20**(3-4), 591–604.

Butler IBŁ, Nesbitt RW, Butler I.B., Nesbitt R.W. (1999) Trace element distributions in the chalcopyrite wall of a black smoker chimney: insights from laser ablation inductively coupled plasma mass spectrometry (LA-ICP-MS). *Earth Planet Sci Lett* **167**(3), 335–345.

Calderón IL, Arenas FA, Pérez JM, Fuentes DE, Araya MA, Saavedra CP, Tantaleán JC, Pichuantes SE, Youderian PA, Vásquez CC (2006) Catalases are NAD(P)H-dependent tellurite reductases. (C Herman, Ed.). *PLoS One* **1**(1), e70.

Candelise C, Winskel M, Gross R (2012) Implications for CdTe and CIGS technologies production costs of indium and tellurium scarcity. *Prog Photovoltaics Res Appl* **20**(6), 816–831.

Challenger F (1945) Biological methylation. *Chem Rev* **36**(3), 315–361.

Chasteen TG, Bentley R (2003) Biomethylation of selenium and tellurium: microorganisms and plants. *Chem Rev* **103**(1), 1–25.

Chasteen TG, Fuentes DE, Tantaleán JC, Vásquez CC (2009) Tellurite: history, oxidative stress, and molecular mechanisms of resistance. *FEMS Microbiol Rev* **33**(4), 820–832.

Claessens PL, White CW (1993) Method of tellurium separation from copper electrorefining slime.

Csotonyi JT, Stackebrandt E, Yurkov V (2006) Anaerobic respiration on tellurate and other metalloids in bacteria from hydrothermal vent fields in the eastern Pacific Ocean. *Appl Environ Microbiol* **72**(7), 4950–4956.

Deuticke B, Lütkemeier P, Poser B (1992) Tellurite-induced damage of the erythrocyte membrane. Manifestations and mechanisms. *Biochim Biophys Acta* **1109**(1), 97–107.

Dostálek (2011) Immobilized biosorbents for bioreactors and commercial biosorbents. “Microb. Biosorption Met.” (Eds P Kotrba, M Mackova, T Macek) pp.285–300. (Springer: New York)

Escobar B, Bustos K, Morales G, Salazar O (2008) Rapid and specific detection of *Acidithiobacillus ferrooxidans* and *Leptospirillum ferrooxidans* by PCR. *Hydrometallurgy* **92**(3-4), 102–106.

Fthenakis VM (2004) Life cycle impact analysis of cadmium in CdTe PV production. *Renew Sustain Energy Rev* **8**(4), 303–334.

Fthenakis VM, Wang W (2004) “Leaching of cadmium, tellurium and copper from cadmium telluride photovoltaic modules progress report.” (Brookhaven National Laboratory: Upton, NY)

Fthenakis VM, Wang W (2006) Extraction and separation of Cd and Te from cadmium telluride photovoltaic manufacturing scrap. *Prog Photovoltaics Res Appl* **14**, 363–371.

Gaultois MW, Sparks TD, Borg CKH, Seshadri R, Bonificio WD, Clarke DR (2013) Data-Driven Review of Thermoelectric Materials: Performance and Resource Considerations. *Chem Mater* **25**(15), 2911–2920.

Green MA (2009) Estimates of Te and In prices from direct mining of known ores. *Prog Photovoltaics Res Appl* **17**(5), 347–359.

Green MA (2011) Learning experience for thin-film solar modules: First Solar, Inc. case study. *Prog Photovoltaics Res Appl* **19**(4), 498–500.

Holden JF, Adams MWW (2003) Microbe–metal interactions in marine hydrothermal environments. *Curr Opin Chem Biol* **7**(2), 160–165.

Homm G, Klar PJ (2011) Thermoelectric materials-compromising between high efficiency and materials abundance. *Phys status solidi - Rapid Res Lett* **5**(9), 324–331.

Jennings PH (1971) Extractive metallurgy of tellurium. “Tellurium.” (Ed WC Cooper) pp.14–53. (Von Nostrand Reinhold Company: New York)

Kraemer D, Poudel B, Feng H-P, Caylor JC, Yu B, Yan X, Ma Y, Wang X, Wang D, Muto A, McEnaney K, Chiesa M, Ren Z, Chen G (2011) High-performance flat-panel solar thermoelectric generators with high thermal concentration. *Nat Mater* **10**(7), 532–8.

Lovley DR, Coates JD (1997) Bioremediation of metal contamination. *Curr Opin Biotechnol* **8**(3), 285–289.

Marwede M, Reller A (2012) Future recycling flows of tellurium from cadmium telluride photovoltaic waste. *Resour Conserv Recycl* **69**, 35–49.

Mirgorodsky AP, Merle-Méjean T, Champarnaud J-C, Thomas P, Frit B (2000) Dynamics and structure of TeO2 polymorphs: model treatment of paratellurite and tellurite; Raman scattering evidence for new γ- and δ-phases. *J Phys Chem Solids* **61**, 501–509.

Okkenhaug G (2010) “Environmental risks regarding the use and final disposal of CdTe PV modules. Document No. 20092155-00-5-R.” (Oslo, Norway)

Ollivier PRL, Bahrou AS, Church TM, Hanson TE (2011) Aeration controls the reduction and methylation of tellurium by the aerobic, tellurite-resistant marine yeast *Rhodotorula mucilaginosa*. *Appl Environ Microbiol* **77**(13), 4610–4617.

Ollivier PRL, Bahrou AS, Marcus S, Cox T, Church TM, Hanson TE (2008) Volatilization and precipitation of tellurium by aerobic, tellurite-resistant marine microbes. *Appl Environ Microbiol* **74**(23), 7163–7173.

Olson GJ, Brierley JA, Brierley CL (2003) Bioleaching review part B: progress in bioleaching: applications of microbial processes by the minerals industries. *Appl Microbiol Biotechnol* **63**(3), 249–257.

Paknikar KM, Rajwade JM, Pethkar A V, Goyal DJ, Bilurkar PG, Mate N V, Road GGA, Peth S, Road T (1997) An integrated chemical-microbiological approach for the disposal of waste thin film cadmium telluride photovoltaic modules. In “Mater. Res. Soc. Fall Meet.,” Boston, MA. Pp 133–138. (Boston, MA)

Patyk A (2009) Thermoelectrics: Impacts on the environment and sustainability. *J Electron Mater* **39**(9), 2023–2028.

Pérez JM, Calderón IL, Arenas FA, Fuentes DE, Pradenas GA, Fuentes EL, Sandoval JM, Castro ME, Elías AO, Vásquez CC (2007) Bacterial toxicity of potassium tellurite: unveiling an ancient enigma. (A Sonenshein, Ed.). *PLoS One* **2**(2), e211.

Pine A, Dresselhaus G (1971) Raman Spectra and Lattice Dynamics of Tellurium. *Phys Rev B* **4**(2), 356–371.

Rajwade JM, Paknikar KM (2003) Bioreduction of tellurite to elemental tellurium by Pseudomonas mendocina MCM B-180 and its practical application. *Hydrometallurgy* **71**(1-2), 243–248.

Rathgeber C, Yurkova N, Stackebrandt E, Beatty JT, Yurkov V, Beatty TJ (2002) Isolation of tellurite- and selenite-resistant bacteria from hydrothermal vents of the

Juan de Fuca Ridge in the Pacific Ocean. *Appl Environ Microbiol* **68**(9), 4613–4622.

Rathgeber C, Yurkova N, Stackebrandt E, Schumann P, Humphrey E, Beatty JT, Yurkov V (2006) Metalloid reducing bacteria isolated from deep ocean hydrothermal vents of the Juan de Fuca Ridge, *Pseudoalteromonas telluritireducens* sp. nov. and *Pseudoalteromonas spiralis* sp. nov. *Curr Microbiol* **53**(5), 449–456.

Reiser F, Rodrigues C, Rosa D (2009) High-technology elements for thin-film photovoltaic applications: a demand-supply outlook on the basis of current energy and PV market growths scenarios. In “5th User Forum Thin-Film Photovoltaics,” Würzburg, Germany. Pp 120–125. (Würzburg, Germany)

Rohwerder T, Gehrke T, Kinzler K, Sand W (2003) Bioleaching review part A: progress in bioleaching: fundamentals and mechanisms of bacterial metal sulfide oxidation. *Appl Microbiol Biotechnol* **63**(3), 239–248.

Sabaty M, Avazéri C, Pignol D, Vermeglio A (2001) Characterization of the reduction of selenate and tellurite by nitrate reductases. *Appl Environ Microbiol* **67**(11), 5122–5126.

Sand W, Rohde K, Sobotke B, Zenneck C (1992) Evaluation of *Leptospirillum ferrooxidans* for leaching. *Appl Environ Microbiol* **58**(1), 85–92.

Schweitzer GK, Pesterfield LL (2010) “The aqueous chemistry of the elements.” (Oxford University Press: New York)

Stafiej JS, Claessens P, White CW (1999) Tellurium extraction from copper electrorefining slimes.

Strem Chemicals Inc. Dimethyl cadmium material safety data sheet. *http://www.strem.com/catalog/v/48-5040/*.

Swearingen JW, Araya M a, Plishker MF, Saavedra CP, Vásquez CC, Chasteen TG (2004) Identification of biogenic organotellurides in *Escherichia coli* K-12 headspace gases using solid-phase microextraction and gas chromatography. *Anal Biochem* **331**(1), 106–114.

Thayer JS (2002) Review: Biological methylation of less-studied elements. *Appl Organomet Chem* **16**(12), 677–691.

Tremaroli V, Fedi S, Zannoni D (2007) Evidence for a tellurite-dependent generation of reactive oxygen species and absence of a tellurite-mediated adaptive response to oxidative stress in cells of Pseudomonas pseudoalcaligenes KF707. *Arch Microbiol* **187**(2), 127–135.

Turner RJ (2001) Tellurite toxicity and resistance in Gram-negative bacteria. *Recent Res Dev Microbiol* **5**, 69–77.

Turner RJ, Aharonowitz Y, Weiner JH, Taylor DE (2001) Glutathione is a target in tellurite toxicity and is protected by tellurite resistance determinants in *Escherichia coli*. *Can J Microbiol* **47**(1), 33–40.

Ullal HS, Roedern B Von (2007) Thin film CIGS and CdTe photovoltaic technologies: commercialization, critical issues, and applications. In “22nd Eur. Photovolt. Sol. Energy Conf. Exhib.,” Milan, Italy. Pp 1–4. (Milan, Italy)

Veglio F, Beolchini F (1997) Removal of metals by biosorption: a review. *Hydrometallurgy* **44**(3), 301–316.

Vetriani C, Chew YS, Miller SM, Yagi J, Coombs J, Lutz RA, Barkay T (2005) Mercury adaptation among bacteria from a deep-sea hydrothermal vent. *Appl Environ Microbiol* **71**(1), 220–226.

Volesky B (2001) Detoxification of metal-bearing effluents: biosorption for the next century. *Hydrometallurgy* **59**(2-3), 203–216.

Wang W, Fthenakis V (2005) Kinetics study on separation of cadmium from tellurium in acidic solution media using ion-exchange resins. *J Hazard Mater* **125**(1-3), 80–88.

Yoon BM, Shim SC, Pyun HC, Lee DS (1990) Hydride generation atomic absorption determination of tellurium species in environmental samples with in situ concentration in a graphite furnace. *Anal Sci* **6**(4), 561–566.

Zweibel K (2010) The impact of tellurium supply on cadmium telluride photovoltaics. *Science (80-)* **328**(5979), 699–701.

Table 1. Soluble tellurium from 0.1 g of various compounds in liquid ASW after 48 h at 37°C

Tellurium source[a]	**Soluble tellurium concentration**[b] **(mmol l^{-1})**
Metallic tellurium	0.038
Tellurium dioxide	0.063
Autoclave slime	0.066
Cadmium telluride	0.001
Bismuth telluride	0.037

[a]Incubated in absence of EPR3

[b]ICP-MS sensitive to 20 nmol l^{-1}

FIGURE CAPTIONS

Figure 1 Raman spectra of standards of metallic tellurium, tellurium dioxide and tellurite (dissolved in solid ASW media) between 100 cm^{-1} and 200 cm^{-1}. The metallic tellurium exhibits distinctive peaks at 122 cm^{-1} and 141 cm^{-1}. The tellurium dioxide exhibits distinctive peaks at 122 cm^{-1}, 149 cm^{-1}, 174 cm^{-1} and 196 cm^{-1}. The tellurite does not exhibit any Raman peaks.

Standards of: (◆) Tellurium dioxide, (■) metallic tellurium, (●) tellurite

Figure 2 Raman spectra of EPR3 precipitations after incubation with tellurium dioxide, metallic tellurium, and tellurite on solid media. Each precipitation exhibits Raman peaks distinctive of metallic tellurium, at 122 cm^{-1} and 141 cm^{-1}. These spectra were recorded from the boxed region shown in Figure 4, suggesting that EPR3 is precipitating metallic tellurium away from the tellurium sources indicated.

EPR3 precipitation - incubation with: (◆) Tellurium dioxide, (■) metallic tellurium, (●) tellurite

Figure 3 ICP-MS results for headspace sampling of tellurium 125 above EPR3. Samples of tellurite, metallic tellurium, tellurium dioxide, autoclave slime, bismuth telluride, and cadmium telluride were incubated aerobically with EPR3 on solid ASW for 48 h. In the headspace of each sample a gaseous tellurium species was detected. In controls of the tellurium compounds incubated on sterile solid ASW without EPR3, zero tellurium counts were detected during the sampling time, meaning no gaseous tellurium was detected.

Gaseous tellurium from: (●) Tellurite, (▲) metallic tellurium, (◆) tellurium dioxide, (■) autoclave slime, (▼) bismuth telluride, (◣) cadmium telluride

Figure 4 a) Photographs of ASW agar plates amended with 0.1 mmol l^{-1} tellurite and inoculated with EPR3. After 48 h, bacterial colonies are dark brown, indicative of metallic tellurium precipitation. The plate was aged an additional 120 h. In these plates the dark brown colonies faded to a lighter brown. b,c) Photographs of EPR3-inoculated ASW plates after addition of b) metallic tellurium and c) tellurium dioxide. The colonies in contact with the tellurium compounds and their surrounding colonies turned dark brown, indicative of metallic tellurium precipitation. Those colonies closest to the tellurium source were darkest brown, fading to lighter brown the further the colonies were from the tellurium source. The boxed region in each sample was extracted for further analysis.

Figure 5 The change in soluble tellurium concentration over time during incubation with EPR3, as measured by ICP-MS. The points on the plot are the average of three replicates and the error bars are the standard deviation of the three measured values. A cubic spline fit line is drawn through the points.

Figure 6 EPR3 precipitation of tellurium from dissolved potassium tellurite, metallic tellurium, and tellurium dioxide over time. a) Photographs of ASW tubes, with the three rightmost samples amended with 0.1 mmol l^{-1} tellurite, 0.1 g tellurium dioxide, and 0.1 g metallic tellurium, then all but the leftmost sample inoculated with EPR3. After 48 h, bacterial colonies exposed to tellurium species are dark brown, indicative of metallic tellurium precipitation. The samples were aged an additional 120 h during which the dark brown colonies faded to a lighter brown for the tellurite and metallic tellurium samples, which at that time resemble the tellurium free EPR3. b) Plot of integrated absorption between 450-800 nm wavelengths as a function of time for the samples.

Note: An ASW sample in which EPR3 precipitated metallic tellurium from telluric acid ($Te(OH)_6$), which is not discussed in this manuscript but was included in the assay, was spliced from the images using Adobe Photoshop CS3, otherwise minimal processing was performed on the images.

Integrated absorbance (450 - 800 nm) for: (●) Cells, (■) TeO_3^{2-}, (◆) TeO_2, (▲) Te^0

Figure 7 Photographs of a) autoclave slime, b) cadmium telluride, and c) bismuth telluride after addition to the center of dishes inoculated with EPR3. After 48 h the surviving cells closest to the tellurium compounds were brown, indicative of metallic tellurium formation. The darkness of the bacteria faded with distance from the tellurium source. The boxed region in each sample was extracted for further analyses. These analyses included: d)Raman spectra of EPR3 precipitations after incubation with bismuth telluride, cadmium telluride, and autoclave slime on solid media. Each precipitation exhibits Raman peaks characteristic of metallic tellurium, at 122 cm^{-1} and 141 cm^{-1}. These spectra were recorded from the boxed region shown in a), b), c), providing further evidence that EPR3 is precipitating metallic tellurium at locations physically separated from these tellurium sources.

EPR3 precipitation - incubation with: (◆) Bismuth telluride, (■) cadmium telluride, (●) autoclave slime.

Figure 8 Schematic of proposed tellurium speciation in a bacterium and its media. Diffusion is represented by solid arrows and chemical changes are represented by hollow arrows. We propose that a solid tellurium source (e.g. tellurium dioxide, autoclave slime, cadmium telluride, and bismuth telluride) dissolves in the media to yield soluble tellurite. The tellurite crosses the cell wall and the bacterium transforms it to either metallic tellurium or a gaseous tellurium species (for instance, dimethyl telluride by way of the Challenger mechanism). While there is undissolved tellurium source, the metallic tellurium - tellurite - volatile tellurium system is in steady state; solid tellurium dissolves to tellurite, which can be converted to a gaseous tellurium species, which escapes to the environment by volatilization. Volatile tellurium species may also be transforming back to tellurite (represented by dotted hollow arrow).

Figure 1

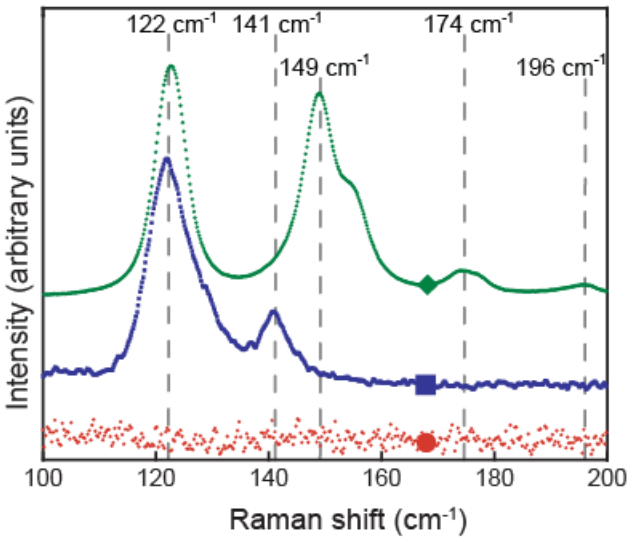
122 cm-1
141 cm-1
149 cm-1
174 cm-1
196 cm-1
Intensity (arbitrary units)
100
120
140
160
180
200
Raman shift (cm-1)

Figure 2.

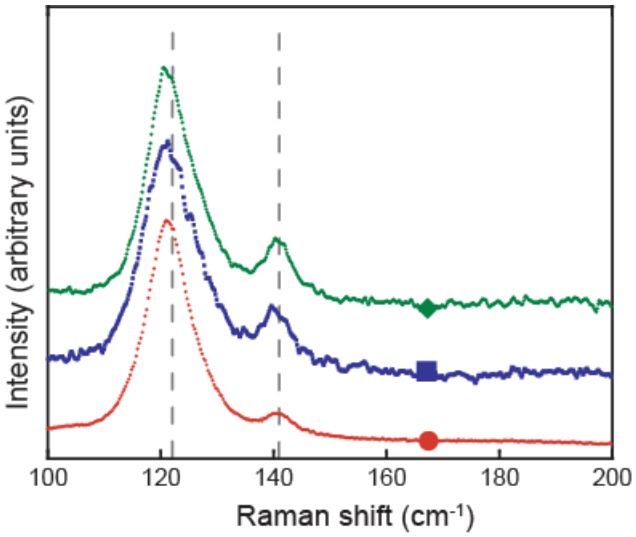
Intensity (arbitrary units)
100
120
140
160
180
200
Raman shift (cm-1)

Figure 3.

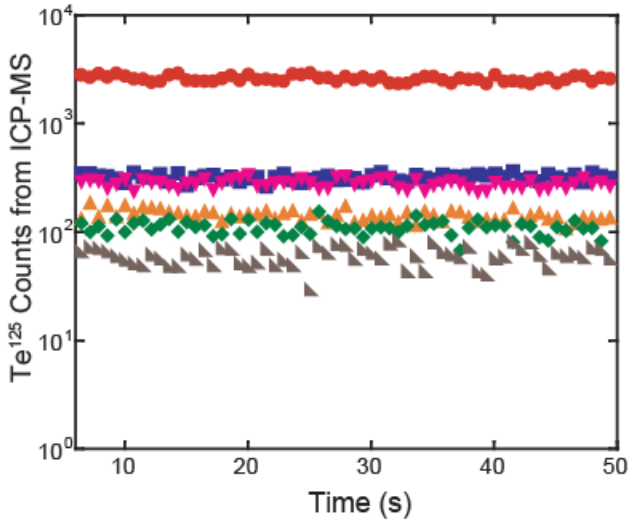
10^4
10^3
10^2
10^1
10^0
Te^{125} Counts from ICP-MS
10
20
30
40
50
Time (s)

Figure 4.

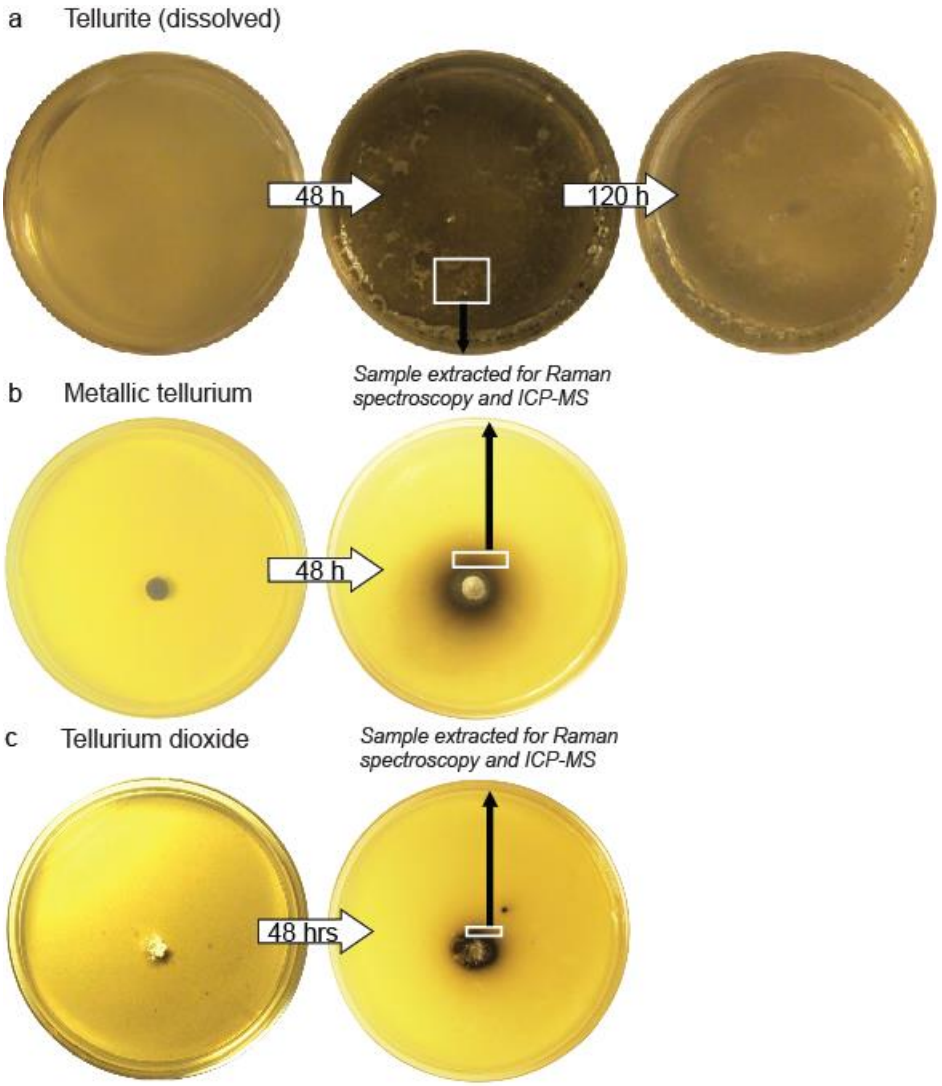
a Tellurite (dissolved)
48 h
120 h
Sample extracted for Raman spectroscopy and ICP-MS
b Metallic tellurium
48 h
c Tellurium dioxide
Sample extracted for Raman spectroscopy and ICP-MS
48 hrs

Figure 5.

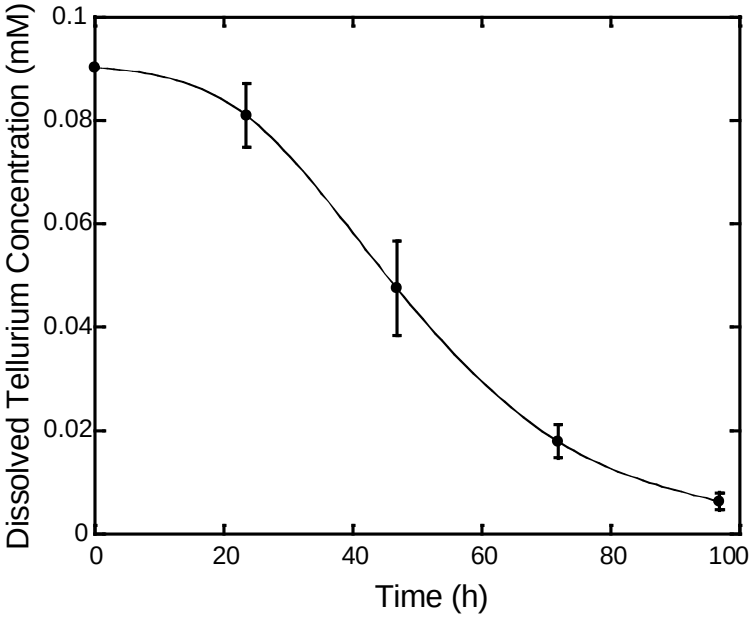
Dissolved Tellurium Concentration (mM)
0.1
0.08
0.06
0.04
0.02
0
0
20
40
60
80
100
Time (h)

Figure 6.

a

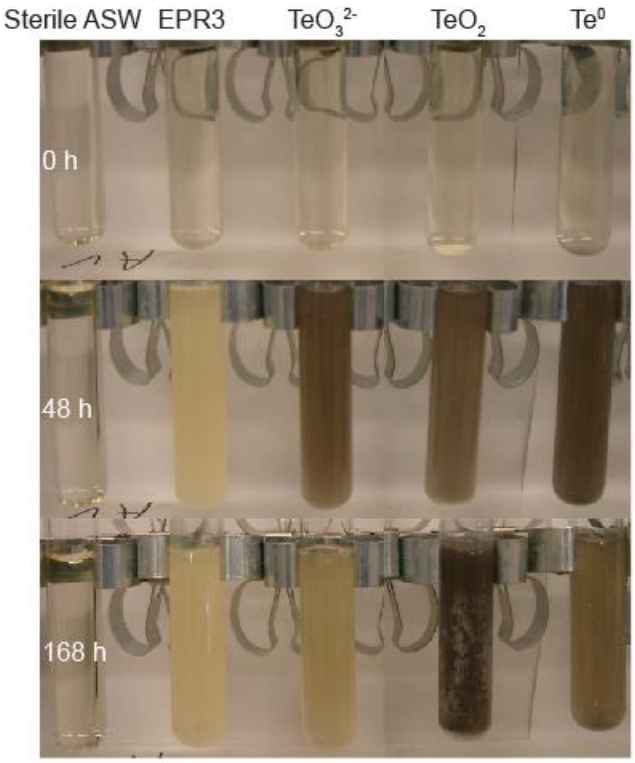
Sterile ASW
EPR3
TeO_3^{2-}
TeO_2
Te^0
0 h
48 h
168 h

b

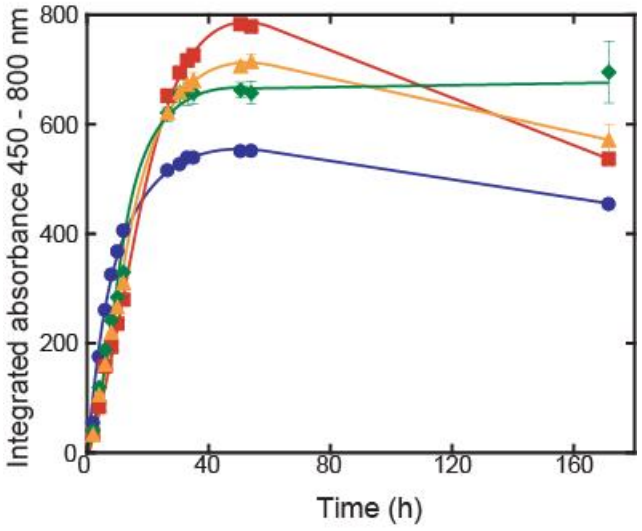
Integrated absorbance 450 - 800 nm
800
600
400
200
0
0
40
80
120
160
Time (h)

Figure 7.

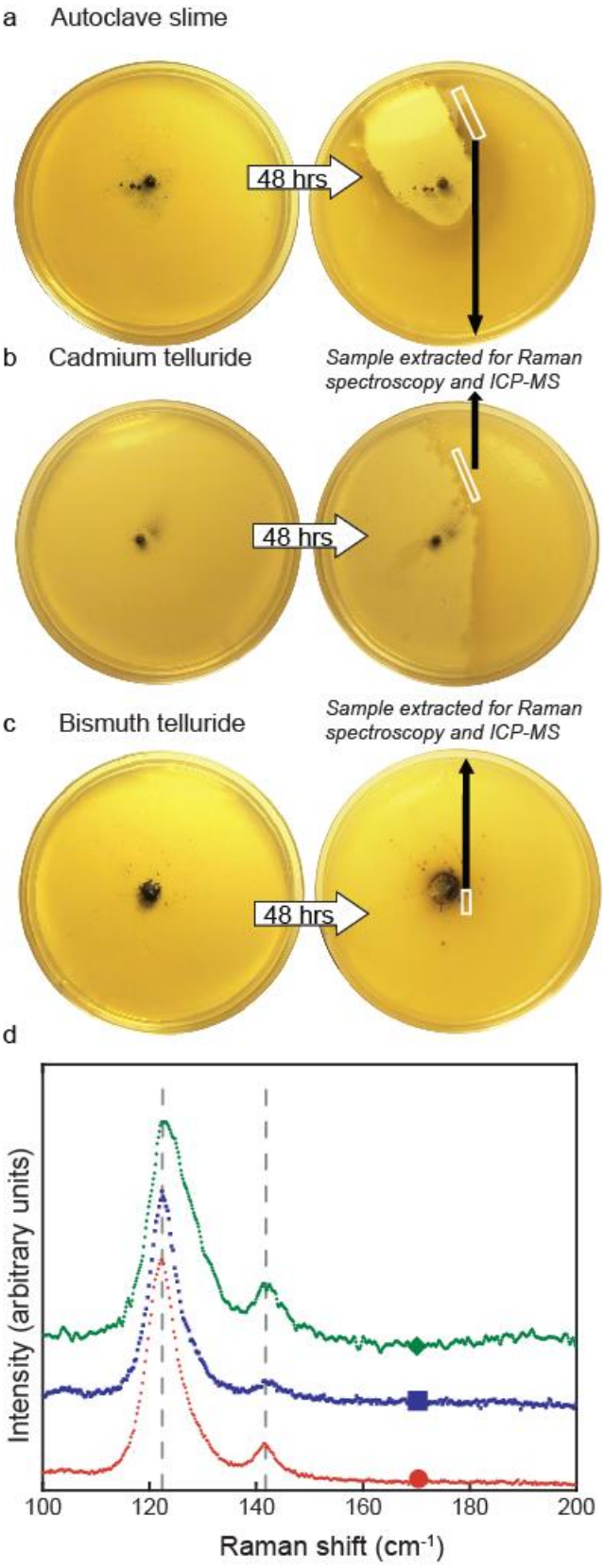
a Autoclave slime
48 hrs
b Cadmium telluride
Sample extracted for Raman spectroscopy and ICP-MS
48 hrs
c Bismuth telluride
Sample extracted for Raman spectroscopy and ICP-MS
48 hrs
d
Intensity (arbitrary units)
100
120
140
160
180
200
Raman shift (cm-1)

Figure 8.

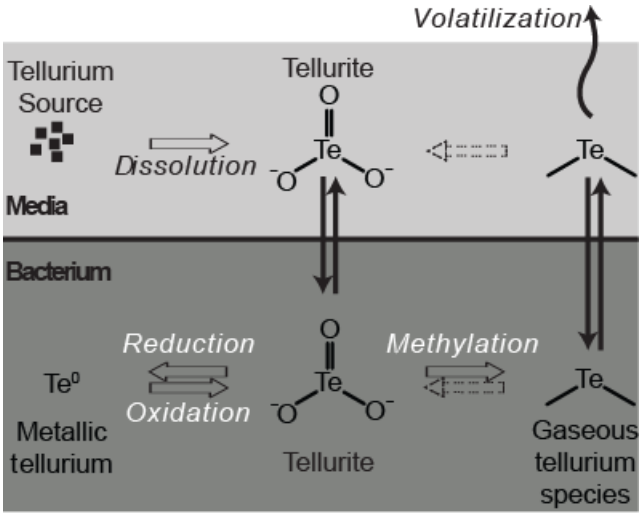
Volatilization
Tellurium Source
Tellurite
Dissolution
Te
Media
Bacterium
Reduction
Methylation
Te⁰
Oxidation
Te
Metallic tellurium
Tellurite
Gaseous tellurium species